Eur. Phys. J. D (2017) 71: 196
DOI: 10.1140/epjd/e2017-80132-8

THE EUROPEAN PHYSICAL JOURNAL D

Regular Article

Existence and switching behavior of bright and dark Kerr solitons in whispering-gallery mode resonators with zero group-velocity dispersion*

Jimmi H. Talla Mbé[1,2,3], Carles Milián[4], and Yanne K. Chembo[5,6,a]

[1] Laboratory of Condensed Matter, Electronics and Signal Processing, Department of Physics, University of Dschang, P.O. Box 67, Dschang, Cameroon
[2] Laboratory of Modelling and Simulation in Engineering, Biomimetics and Prototypes, Department of Physics, University of Yaoundé I, P.O. Box 812, Yaoundé, Cameroon
[3] African Center of Excellence for Information and Communication Technologies (CETIC), Polytechnic School of Yaoundé, P.O. Box 8390, Yaoundé, Cameroon
[4] Centre de Physique Théorique, CNRS, Ecole Polytechnique, 91128 Palaiseau, France
[5] Optics Department, FEMTO-ST Institute, CNRS & Univ. Bourgogne-Franche-Comté, 15B Avenue des Montboucons, 25030 Besançon Cedex, France
[6] GeorgiaTech-CNRS Joint International Laboratory [UMI 2958], Atlanta Mirror Lab, School of Electrical and Computer Engineering, 777 Atlantic Dr NW, Atlanta, GA 30332-0250, USA

Received 27 February 2017 / Received in final form 10 May 2017
Published online 19 July 2017 –

Abstract. We use the generalized Lugiato-Lefever model to investigate the phenomenon of Kerr optical frequency comb generation when group-velocity dispersion is null. In that case, the first dispersion term that plays a leading role is third-order dispersion. We show that this term is sufficient to allow for the existence of both bright and dark solitons. We identify the areas in the parameter space where both kind of solitons can be excited inside the resonator. We also unveil a phenomenon of hysteretic switching between these two types of solitons when the power of the pump laser is cyclically varied.

1 Introduction

The topic of Kerr optical frequency comb using ultra-high Q whispering gallery mode resonators has been the focus of extensive research in recent years [1,2]. These combs are obtained after pumping these Kerr-nonlinear cavities with a resonant continuous-wave (CW) laser. Above a certain threshold, the small volume of confinement, high photon density and long photon lifetime contribute to the excitation of the neighboring cavity eigenmodes through four-wave mixing (FWM) interactions of the kind $\hbar\omega_m + \hbar\omega_p \rightarrow \hbar\omega_n + \hbar\omega_q$, where two input photons m and p interact coherently via the Kerr nonlinearity to yield two output photons n and q. This FWM induces a global coupling between the modes, which potentially results in the excitation of up to several hundred spectral lines. This cascade of photonic interactions yields the so-called Kerr optical frequency comb, which is a set of equidistant spectral components in the Fourier domain. Many features of the nonlinear and quantum properties of these combs have already been analyzed in depth in several research works [3–12]. From the applications standpoint, Kerr combs have been found to be of particular relevance in many areas, including aerospace and telecommunication engineering, spectroscopy, and microwave/lightwave frequency synthesis [13–25].

It is noteworthy that Kerr comb generation requires the frequency shift generated by self-phase modulation (SPM) to be compensated by both the laser frequency detuning and the overall (chromatic and geometric) dispersion of the resonator. From this requirement, one can foreshadow the central role that dispersion plays in the Kerr comb generation process. In general, studies in Kerr optical frequency comb generation only focus on the two distinct signs for the second-order dispersion parameter (also known as group-velocity dispersion, or GVD), referred to as normal (positive GVD) and anomalous (negative GVD) dispersion regimes. Kerr comb generation in both regimes has been the focus of a large amount of research work, that has allowed to identify the various possible solutions arising in each case, and which include rolls (also referred to as Turing patterns), spatiotemporal chaos, and solitons of various forms: bright/dark, breathers, and molecules [11,26]. Bright solitons are usually found

* Contribution to the Topical Issue "Theory and Applications of the Lugiato-Lefever Equation", edited by Yanne K. Chembo, Damia Gomila, Mustapha Tlidi, Curtis R. Menyuk.

[a] e-mail: yanne.chembo@femto-st.fr

in the anomalous dispersion regime [11,21,26], in contrast to dark solitons that are generally obtained in the normal dispersion regime [11,27–33].

However, the case of zero GVD has not been analyzed in depth, despite its relevance from a bifurcation analysis point of view. On the one hand, it is well known that very small GVD is desirable in order to obtain broadband combs, and therefore it is important to analyze what occurs when second-order dispersion is strictly null, as this permits to understand how the system behaves asymptotically on each side of the zero-GVD limit [34]. On the other hand, when the second-order dispersion term is null, the higher orders of dispersion should be considered and in this case the third-order dispersion (or TOD) plays the leading role. In both cases, the spectro- and spatio-temporal properties of the comb display some singular features that are still to be investigated and understood in depth.

By setting the pump exactly at the zero GVD, all excited comb lines fall in the normal (anomalous) if blue (red)-shifted from the pump. Any soliton (bright or dark) formed around the pump is strongly affected by the recoil effect, associated to the resonant radiation tail, which helps locating the soliton core firmly in the normal or anomalous GVD for bright or dark solitons, respectively (see Ref. [34] for the case of a bright soliton in the anomalous GVD and the pump under the normal GVD). Therefore, under these conditions, the existence of both bright and dark solitons is highly expected, and indeed possible.

In this article, we aim to address this problem, and analyze the dynamical properties of soliton Kerr combs when GVD is null. The structure of the article is therefore the following. In the next section, we present the model under investigation, which is a generalized Lugiato-Lefever equation. Section 3 is devoted to the case of null overall dispersion, where only flat states are allowed. We then analyze in Section 4 the effect of third-order dispersion, which is the first dispersion term to be accounted for when GVD is null. The last section concludes the article.

2 Model

Kerr comb generation is usually investigated using the mean-field Lugiato-Lefever equation (LLE), which was first introduced in reference [35]. It was shown for the first time in reference [36] that the LLE could be used to study the dynamics of laser fields confined in dissipative and dispersive ring-cavities. Later on, the LLE was used to provide an accurate insight into the intra-cavity spatiotemporal dynamics of Kerr comb generators [5–7]. Explicitly, in a dimensionless form, the generalized LLE for Kerr comb generation can be written as

$$\frac{\partial\psi}{\partial t} = F - (1+i\alpha)\psi + i|\psi|^2\psi + i\sum_{n=2}^{n_{\max}} i^n \frac{b_n}{n!}\frac{\partial^n\psi}{\partial\theta^n}, \quad (1)$$

where the variable $\psi(\theta,t)$ stands for the complex slowly-varying envelope of the total intracavity field. The dimensionless time t is scaled with regards to $2\tau_{\rm ph}$, where $\tau_{\rm ph} = 1/\Delta\omega_{\rm tot}$ is the photon lifetime of the loaded cavity and $\Delta\omega_{\rm tot}$ is the total (or loaded) linewidth of the pumped resonance. The variable $\theta \in [-\pi,\pi]$ stands for the azimuthal angle along the circumference of the resonator.

The dimensionless LLE has periodic boundary conditions in the angular variable and is characterized by the parameters F (pump), α (frequency detuning), and b_n (dispersion parameters at the nth order, with $2 \leq n \leq n_{\max}$). More specifically, the dimensionless and real-valued pump field F is related to the pump power P (in watts) as $F = [8g_0\Delta\omega_{\rm ext}/\Delta\omega_{\rm tot}^3]^{\frac{1}{2}}[P/\hbar\omega_{\rm las}]^{\frac{1}{2}}$, where $\omega_{\rm las}$ is the laser angular frequency, $g_0 = n_2 c\hbar\omega_{\rm las}^2/n_0^2 V_0$ is the nonlinear gain with n_0 and n_2 being respectively the linear and nonlinear refraction indices of the bulk material, V_0 is the effective volume of the pumped mode, c is the velocity of light in vacuum, $\hbar$ is the reduced Planck constant, while $\Delta\omega_{\rm ext}$ is the external (or coupling) linewidth of the pumped resonance. The detuning parameter is $\alpha = -2\sigma/\Delta\omega_{\rm tot}$, where $\sigma = \omega_{\rm las} - \omega_{\rm res}$ is the difference between the pump laser and the cold-cavity resonance angular frequencies. Finally, the nth order dispersion parameters can be expressed as $b_n = 2v_g\tau_{\rm ph}\beta_n\Omega_{\rm FSR}^n$, where v_g is the group velocity in the bulk material at the pump laser frequency, $\Omega_{\rm FSR}$ is the angular free-spectral range (FSR) of the resonator, and β_n is the nth order dispersion coefficient as usually defined in optical materials. It is also important to note that the intracavity power in watts can be simply recovered as $|E|^2 = [\hbar\omega_{\rm las}/2g_0\tau_{\rm ph}T_{\rm FSR}]|\psi|^2$, where $T_{\rm FSR} = 2\pi/\Omega_{\rm FSR}$ is the intracavity round-trip time. For crystalline disk-resonators, the photon lifetime $\tau_{\rm ph}$ can be longer than 1 μs (see Refs. [37–40]) while it is of the order of few ns for integrated resonators. The GVD and TOD respectively correspond to b_2 and b_3. By convention, the anomalous GVD regime is defined by $b_2 < 0$ while normal GVD corresponds to $b_2 > 0$.

It is known that the LLE can describe the dynamics of the intracavity field with outstanding precision. For example, in reference [9], the experimental spectra involved more than 300 modes, and where shown to agree with the theoretical one over a dynamical range greater than 80 dB. We will investigate in the next sections these dispersion parameters on the spatio-temporal dynamics of the intracavity field.

3 Dynamics of the system with null overall dispersion

The dynamics of the resonator when the overall dispersion is null is obtained by uniformly setting the dispersion terms b_n to zero in equation (1). The equilibria $\psi_{\rm e}$ are obtained by setting the temporal derivative to zero as well, and they are solutions of the following nonlinear algebraic equation:

$$F^2 = \rho^3 - 2\alpha\rho^2 + (\alpha^2+1)\rho \equiv G(\alpha,\rho), \quad (2)$$

with $\rho = |\psi_{\rm e}|^2$ being the intracavity power at equilibrium. Because they are independent of time and space, the equilibria $\psi_{\rm e}$ are homogenous steady state solutions

which are represented by a single spectral line in the Fourier domain. The extrema of the function $G(\alpha, \rho)$ are

$$F_{\pm}^2 = G\left[\alpha, \rho_{\mp}(\alpha)\right] = \frac{2}{27}\left[\alpha\left(\alpha^2+9\right) \pm \sqrt{\left(\alpha^2-3\right)^3}\right] \quad (3)$$

with $\rho_{\mp}(\alpha) = [2\alpha \mp \sqrt{\alpha^2-3}]/3$. For a given pump intensity F^2, equation (2) shows that we have only one equilibrium if $\alpha < \sqrt{3}$, but up to three equilibria $\rho_{\rm d} < \rho_{\rm i} < \rho_{\rm u}$ when $\alpha > \sqrt{3}$, with the subscripts d, i and u standing for down, intermediate and up, respectively. It is well known that the down- and uppermost solutions are stable, while the intermediate one is unstable (see, e.g., Refs. [11,41] for a thorough analysis of the flat state solutions).

In order to analyze the stability of these equilibria, it is convenient to explicitly split ψ into its real and imaginary parts so that equation (1) can be rewritten under the form of a two-dimensional flow with real variables. The eigenvalues of the corresponding Jacobian matrix around the flat-states are given by:

$$\lambda_{\pm} = -1 \pm \sqrt{1 - \frac{\partial G}{\partial \rho}} = -1 \pm \sqrt{(3\rho - \alpha)(\alpha - \rho)}. \quad (4)$$

The analysis of these eigenvalues reveals that no local bifurcation can occur in the system except when $\rho = \rho_{\pm}$ since, as one of the eigenvalues is laying on the imaginary axis ($\lambda_+ = 0$) and the second has a negative real part ($\lambda_- < 0$). The equilibria are therefore non-hyperbolic in this case.

For a pump field such that $F_-^2 < F^2 < F_+^2$, the system is driven in the hysteresis area. The asymptotic flat state will emerge from a competition between $\rho_{\rm d}$ and $\rho_{\rm u}$, which are both stable attractors. In fact, the final state will critically depend on the value F^2 of the pump with regards to the median pump power:

$$F_{\rm m}^2 = \frac{1}{2}\left(F_-^2 + F_+^2\right) = \frac{2\alpha(\alpha^2+9)}{27}. \quad (5)$$

For a pump $F < F_{\rm m}$, the amplitude of the flat state will be $\rho_{\rm d}$, while for $F > F_{\rm m}$, the system will converge to $\rho_{\rm u}$. This phenomenology, which is described in Figure 1b, predicts that perturbations to the singular problem of null dispersion will strongly depend on the value of the pump F^2 with regards to the median power $F_{\rm m}^2$.

In the next section, we will investigate the effect of TOD when GVD is still null, and analyze the deviation form of the singular manifolds in the spatiotemporal domain.

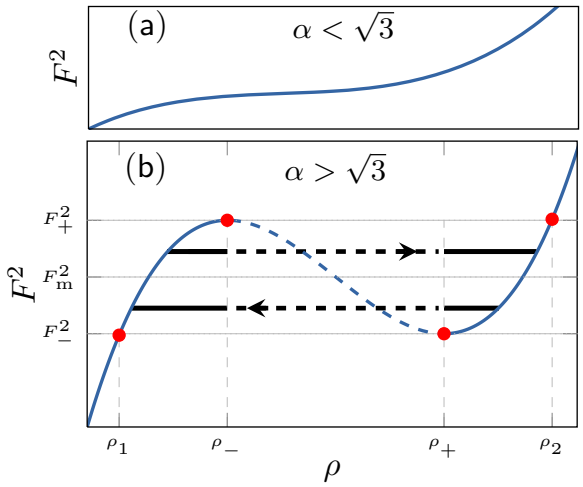

Fig. 1. Laser pump versus the stable equilibrium point of the intra-cavity energy. The analytical values are plotted from equation (2). For (a), $\alpha < \sqrt{3}$: only one stable equilibrium. For (b), $\alpha > \sqrt{3}$: two stable (solid curve) and one unstable (dotted curve) equilibrium points. The attractive curve $\rho_{\rm d}$ represents all the values of ρ lower than ρ_- whereas, the attractive curve $\rho_{\rm u}$ represents all the values of ρ greater than ρ_+. The solid parts of the arrows is used to emphasize on the fact that one among $\rho_{\rm u}$ and $\rho_{\rm d}$ can be more attractive than other (the solid part is longer in the side of attractive line), becoming therefore the final predominant amplitude of the flat state. The dash part of an arrow emphasizes on the unstable equilibrium $\rho_{\rm i}$. The axis ticks have been removed for a general interpretation. But, in (a), $\alpha = 1.5$ while for (b) $\alpha = 3.5$.

4 Bright and dark solitons in the presence of third-order dispersion

We now consider equation (1) when all the dispersion coefficients are equal to zero, except the TOD coefficient b_3.

The effect of TOD on dissipative structures has already been analyzed in several research works. Some of these investigations were focused on the reversibility breaking in the system which is responsible for the soliton drift, while other works analyzed specific solutions such as time-varying solitons [34,42–47]. It is important to note that owing to geometrical dispersion, the overall dispersion of a resonator can in some cases be engineered via its shape to yield a dispersion profile closely corresponding to arbitrary configurations [48–53].

When TOD is accounted for, non-trivial states may arise in the system close to, or inside the hysteresis area. In particular, for a pump selected at a particular median value $F_{\rm m} = 1.68$ or just around it, the system preferably converges towards a cavity soliton instead of flat states. Bright and dark solitons yielding Kerr combs with single-FSR spacing are obtained. The spatiotemporal profiles and the corresponding spectra are displayed in Figure 2. Despite the fact that the type of soliton (bright or dark) depends on the initial condition, bright cavity solitons are preferably obtained when the pump is below $F_{\rm m}$, whereas dark cavity solitons preferably emerge in the opposite case.

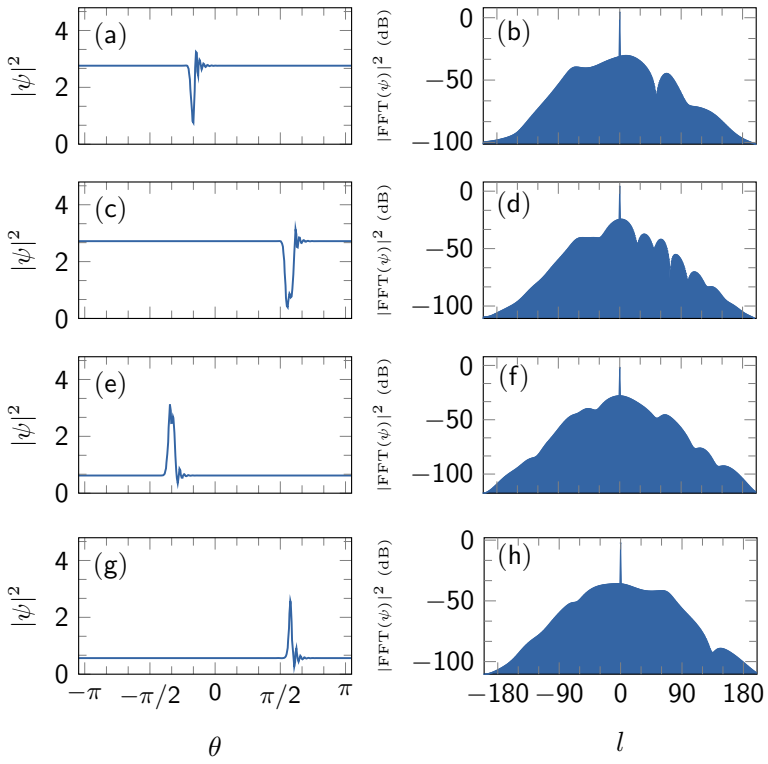

Fig. 2. Soliton spatial waveforms (left column) and the corresponding frequency combs (right column) for the pump around $F_\mathrm{m} = 1.68$. As the pump is monitored from 1.72 ((a) and (b)) to 1.64 ((g) and (h)), the soliton waveform changes as well from for both dark and bright cavity solitons. The frequency combs have a single-FSR spacing, but their amplitudes undergo some changes ((b), (d), (f), (h)). For these plots, $b_3 = 4.08 \times 10^{-5}$, $\alpha = 2.5$, ((a) and (b)) $F = 1.72$, ((c) and (d)) $F = 1.69$, ((e) and (f)) $F = F_m$ and ((g) and (h)) $F = 1.64$.

For pump values far away from F_m, the system asymptotically converges to a flat state.

Some spatial and spectral profiles of solitons are displayed in Figure 2. Previous works demonstrated that large values of the TOD had the effect of stabilizing the frequency combs [34,46,54] even in the presence of Raman scattering [55].

In order to investigate the branches of stable solitons that can emerge in the system, it is convenient to define a norm that can unambiguously discriminate a soliton from the trivial flat state. There are indeed various ways to define such a norm, but one of the simplest is the following:

$$\mathsf{N} \equiv \int_{-\pi}^{+\pi} |\psi_\mathrm{s} - \psi_\mathrm{e}| \, d\theta, \tag{6}$$

where $\psi_\mathrm{s}(\theta)$ is the soliton spatial profile along the resonator and ψ_e are the equilibria of equation (1). Figure 3 shows the variation of this soliton norm N as a function of the pump field F, for bright and dark solitons with $b_3 > 0$.

Figure 3 also indicates that the solitons can become unstable via an hysteretic path. As a consequence, we can excite the solitons of the same type (bright or dark) with two different amplitudes depending on initial conditions. It can also be seen that bright and dark solitons can be excited with the same parameter values: for a given TOD and conserving the same value of the parameters F and

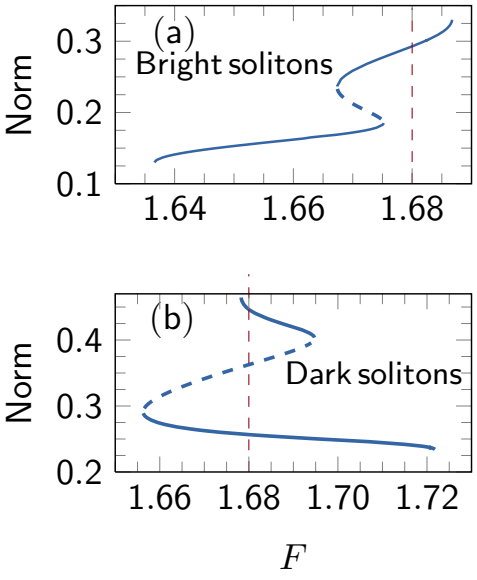

Fig. 3. Soliton norm branches as a function of the pump field for (a) bright and (b) dark solitons when the pump wavelength is exactly set at the zero GVD value ($b_2 = 0$). The only higher-order dispersion term accounted for is TOD with $b_3 = 4.08 \times 10^{-5}$ and $\alpha = 2.5$. Solid (dashed) curves indicate stable (unstable) branches. The vertical dashed lines marks $F = F_\mathrm{m} = 1.68$. The plots are performed using the Newton-Raphson method.

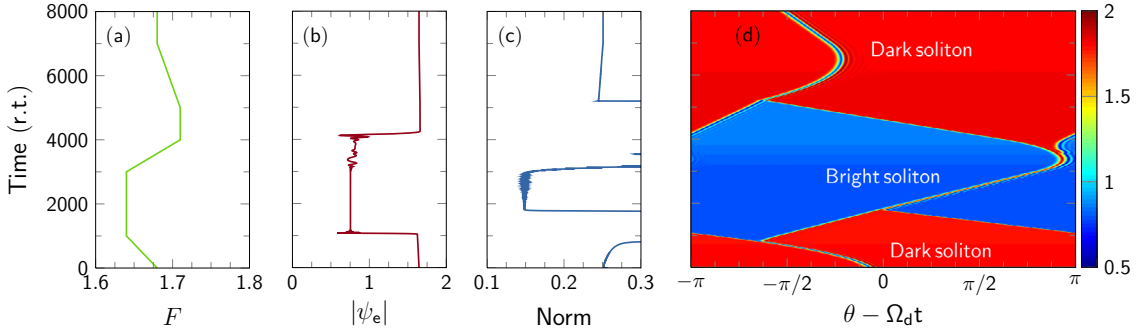

Fig. 4. Soliton switching amongst various branches when the pump power is cyclically varied. The vertical axis of all figures is time in units of round-trips (r.t.). (a) Variations of the pump field F. (b) Variations of the flat state ψ_e. (c) Variations of the norm N. (d) Color-coded intracavity field intensity, showing the various soliton branches (once the drift Ω_d is removed).

α, the cavity can display bright or dark soliton depending on the initial condition. For instance, at $F = 1.68$, stable bright soliton can be recovered (Fig. 3a) as well as stable dark soliton (Fig. 3b). As suggested in references [31–33], the appropriate way to understand why both bright and dark solitons can be excited consists in analyzing the switching waves connecting the homogeneous steady state solutions ρ_d and ρ_u, where ρ_d and ρ_u (with $\rho = |\psi_e|^2$) are the stable flat states. The existence of both bright and dark solitons was already demonstrated in the regime of normal GVD, and attributed to a joint contribution of the third-order dispersion and large detuning [33].

We note here that the existence of both stable bright and dark solitons brings interesting dynamical features to the system. This is illustrated in Figure 4a, where the pump, F is changed with time. The initial state of the resonator is given by the dark soliton at $F = 1.68$ and norm $\simeq$0.25 (see branch in Fig. 4b). As time goes on, F is decreased and the initial dark soliton now follows a path in a branch (a signature of this phenomenology is the soliton velocity change with F) until the pump falls outside the existence limit defined by this branch. At this point, because bright solitons do exist for when dark solitons do not, the dark pulse bifurcates to a bright soliton of norm $\simeq$0.15. At this point, F is increased and swept through the bright soliton branch until it crosses the existence limit for bright solitons. Here again, because dark solitons can still exist when bright ones do not, the bright pulse bifurcates back to the dark soliton found for $F = 1.71$ and norm $\simeq$0.22. The pump is decreased until the initial value of $F = 1.68$, thereby closing the loop.

At the dark-to-bright (bright-to-dark) soliton transitions, the background field switches from the upper to the lower (lower to upper) states of the WGM resonator Figure 4b. As shown in Figure 4b, an interesting feature of this effects is that background switching occurs within a significantly narrower range for the pump powers, F, than that defining the bistability loop of the flat states. Additionally, while the pump range to achieve switching is small, the intensity difference between upper and lower states is kept high, i.e., the bistability loop may be made narrow in F but it comes at the price of diminishing the contrast between upper and lower states. Figure 4c shows

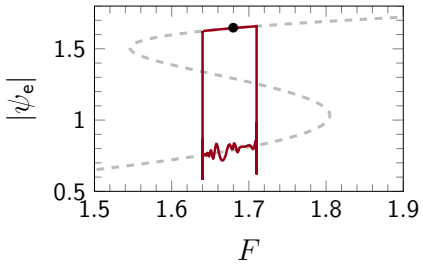

Fig. 5. Hysteretic cycle (in red) completed by $|\psi_e|$ as F is periodically ramped up and down. The temporal dynamics of both variables is exactly the one displayed in Figures 4a and 4b. In the figure, the cycle begins on the black dot and goes counterclockwise. The gray dashed line corresponds to the relationship defined by equation (2) between the pump field and the flat states.

how the norm changes with the cyclic pump variation, while Figure 4d displays the intracavity field. The color-coded representation of this field enables to identify unambiguously the various soliton branches that can be excited in the system.

We can gain even better understanding of the phenomena presented in Figure 4 by plotting the variation of the background flat state $|\psi_e|$ as a function of the cyclically varying pump field F. This representation is displayed in Figure 5, where the hysteretic cycle can be explicitly identified.

5 Conclusion

In this work, we have investigated the dynamics of Kerr optical frequency combs when the group-velocity dispersion is set to zero. We have demonstrated that third-order dispersion is sufficient to lead to the emergence of both bright and dark solitons. These solitons have been shown to exist in a range around an optimal value of the pump power that has been analytically defined. We have also analyzed the hysteretic switching between both types of solitons when the pump power is cyclically varied. Future work will focus on the consideration of other effects such as Raman scattering, pulsed-pumping schemes

or higher-order dispersion [41,56–62] when the system is still very close or at zero group velocity dispersion. This research will enable the community to understand better how the Kerr comb span can be expanded to its maximum extent with the smallest energy footprint possible.

J.H.T.M. acknowledges financial support the African-German Network of Excellence in Science (AGNES). Y.K.C. would like to acknowledge financial support from the European Research Council (ERC) through the project NextPhase, from the Centre National d'Etudes Spatiales (CNES) through the project SHYRO, from the Région de Franche-Comté through the project CORPS, and from the Labex ACTION.

Author contribution statement

J.H.T.M. and C.M. performed the numerical simulations. Y.K.C. conceived and supervised the research project. All authors discussed the results and wrote the article.

References

1. T.J. Kippenberg, R. Holzwarth, S.A. Diddams, Science **322**, 555 (2011)
2. Y.K. Chembo, Nanophotonics **5**, 214 (2016)
3. Y.K. Chembo, D.V. Strekalov, N. Yu, Phys. Rev. Lett. **104**, 103902 (2010)
4. Y.K. Chembo, N. Yu, Phys. Rev. A **82**, 033801 (2010)
5. A.B. Matsko, A.A. Savchenkov, W. Liang, V.S. Ilchenko, D. Seidel, L. Maleki, Opt. Lett. **36**, 2845 (2011)
6. Y.K. Chembo, C.R. Menyuk, Phys. Rev. A **87**, 053852 (2013)
7. S. Coen, H.G. Randle, T. Sylvestre, M. Erkintalo, Opt. Lett. **38**, 37 (2013)
8. A. Coillet, Y.K. Chembo, Opt. Lett. **39**, 1529 (2014)
9. A. Coillet, Y.K. Chembo, Chaos **24**, 013313 (2014)
10. A. Coillet, J. Dudley, G. Genty, L. Larger, Y.K. Chembo, Phys. Rev. A **89**, 013835 (2015)
11. C. Godey, I.V. Balakireva, A. Coillet, Y.K. Chembo, Phys. Rev. A **89**, 063814 (2014)
12. Y.K. Chembo, Phys. Rev. A **93**, 033820 (2016)
13. P. Del'Haye, A. Schliesser, A. Arcizet, R. Holzwarth, T.J. Kippenberg, Nature **450**, 1214 (2007)
14. J.S. Levy, A. Gondarenko, M.A. Foster, A.C. Turner-Foster, A.L. Gaeta, M. Lipson, Nat. Photon. **4**, 37 (2010)
15. F. Ferdous, H. Miao, D.E. Leaird, K. Srinivasan, J. Wang, L. Chen, L.T. Varghese, A.M. Weiner, Nat. Photon. **5**, 770 (2011)
16. J. Li, H. Lee, T. Chen, K.J. Vahala, Phys. Rev. Lett. **109**, 233901 (2012)
17. P. Del'Haye, S.B. Papp, S.A. Diddams, Phys. Rev. Lett. **109**, 263901 (2012)
18. J. Pfeifle et al., Nat. Photon. **8**, 375 (2014)
19. S.B. Papp, K. Beha, P. Del'Haye, F. Quinlan, H. Lee, K.J. Vahala, S.A. Diddams, Optica **1**, 10 (2014)
20. P. Del'Haye, K. Beha, S.B. Papp, S.A. Diddams, Phys. Rev. Lett. **112**, 043905 (2014)
21. T. Herr, V. Brasch, J.D. Jost, C.Y. Wang, N.M. Kondratiev, M.L. Gorodetsky, T.J. Kippenberg, Nat. Photon. **8**, 145 (2014)
22. J. Pfeifle, A. Coillet, R. Henriet, K. Saleh, P. Schindler, C. Weimann, W. Freude, I.V. Balakireva, L. Larger, C. Koos, Y.K. Chembo, Phys. Rev. Lett. **114**, 093902 (2015)
23. S.-W. Huang, J. Yang, J. Lim, H. Zhou, M. Yu, D.-L. Kwong, C.W. Wong, Sci. Rep. **5**, 13355 (2015)
24. K. Saleh, Y.K. Chembo, Opt. Express **24**, 25043 (2016)
25. K. Saleh, Y.K. Chembo, IEEE Photon. J. **8**, 5501807 (2016)
26. P. Parra-Rivas, D. Gomila, M.A. Matias, S. Coen, L. Gelens, Phys. Rev. A **89**, 043813 (2014)
27. W. Liang, A.A. Savchenkov, V.S. Ilchenko, D. Eliyahu, D. Seidel, A.B. Matsko, L. Maleki, Opt. Lett. **39**, 2920 (2014)
28. S.-W. Huang, H. Zhou, J. Yang, J.F. McMillan, A. Matsko, M. Yu, D.-L. Kwong, L. Maleki, C.W. Wong, Phys. Rev. Lett. **114**, 053901 (2015)
29. X. Xue, Y. Xuan, Y. Liu, P.-H. Wang, S. Chen, J. Wang, D.E. Leaird, M. Qi, A.M. Weiner, Nat. Photon. **9**, 594 (2015)
30. V.E. Lobanov, G. Lihachev, T.J. Kippenberg, M.L. Gorodetsky, Opt. Express **23**, 7713 (2015)
31. P. Parra-Rivas, D. Gomila, E. Knobloch, S. Coen, L. Gelens, Opt. Lett. **41**, 2402 (2016)
32. P. Parra-Rivas, E. Knobloch, D. Gomila, L. Gelens, Phys. Rev. A **93**, 063839 (2016)
33. P. Parra-Rivas, D. Gomila, L. Gelens, arXiv:1609.08819 (2016)
34. C. Milian, D.V. Skryabin, Opt. Express **22**, 3732 (2014)
35. L.A. Lugiato, R. Lefever, Phys. Rev. Lett. **58**, 2209 (1987)
36. M. Haelterman, S. Trillo, S. Wabnitz, Opt. Commun. **91**, 410 (1992)
37. A. Coillet, R. Henriet, K.P. Huy, M. Jacquot, L. Furfaro, I. Balakireva, L. Larger, Y.K. Chembo, J. Vis. Exp. **78**, e50423 (2013)
38. G. Lin, S. Diallo, R. Henriet, M. Jacquot, Y.K. Chembo, Opt. Lett. **39**, 6009 (2014)
39. R. Henriet, G. Lin, A. Coillet, M. Jacquot, L. Furfaro, L. Larger, Y.K. Chembo, Opt. Lett. **40**, 1567 (2015)
40. G. Lin, Y.K. Chembo, Opt. Express **23**, 1594 (2015)
41. I.V. Barashenkov, Yu.S. Smirnov, Phys. Rev. E **54**, 5707 (1996)
42. M. Tlidi, A. Mussot, E. Louvergneaux, G. Kozyreff, A.G. Vladimirov, M. Taki, Opt. Lett. **32**, 662 (2007)
43. M. Tlidi, L. Gelens, Opt. Lett. **35**, 306 (2010)
44. M. Taki, A. Mussot, A. Kudlinski, E. Louvergneaux, M. Kolobov, M. Douay, Phys. Lett. A. **374**, 691 (2010)
45. M. Tlidi, L. Cherbi, A. Hariz, S. Coulibaly, Phys. Rev. A **88**, 035802 (2013)
46. P. Parra-Rivas, D. Gomila, F. Leo, S. Coen, L. Gelens, Opt. Lett. **39**, 2971 (2014)
47. F. Leo, S. Coen, P. Kockaert, P. Emplit, M. Haelterman, A. Mussot, M. Taki, Phys. Lett. A **379**, 1934 (2015)
48. I.S. Grudinin, L. Baumgartel, N. Yu, Opt. Express **20**, 6604 (2012)
49. L. Zhang, C. Bao, V. Singh, J. Mu, C. Yang, A.M. Agarwal, L.C. Kimerling, J. Michel, Opt. Lett. **38**, 5122 (2013)
50. L. Zhang, J. Mu, V. Singh, A.M. Agarwal, L.C. Kimerling, J. Michel, IEEE J. Sel. Top. Quantum Electron. **20**, 5900207 (2014)
51. S. Wang, H. Guo, X. Bai, X. Zeng, Opt. Lett. **39**, 2880 (2014)

52. C. Bao, C. Yang, Phys. Rev. A **92**, 023802 (2015)
53. I.S. Grudinin, N. Yu, Optica **2**, 221 (2015)
54. S. Wang, X. Zeng, arXiv:1511.03023 (2015)
55. C. Milian, A.V. Gorbach, M. Taki, A.V. Yulin, D.V. Skryabin, Phys. Rev. A **92**, 033851 (2015)
56. K. Luo, Y. Xu, M. Erkintalo, S. Murdoch, Opt. Lett. **40**, 427 (2015)
57. Y.K. Chembo, I.S. Grudinin, N. Yu, Phys. Rev. A **92**, 043818 (2015)
58. C. Bao, L. Zhang, L.C. Kimerling, J. Michel, C. Yang, Opt. Express **23**, 18665 (2015)
59. G. Lin, S. Diallo, J.M. Dudley, Y.K. Chembo, Opt. Express **24**, 14880 (2016)
60. G. Lin, Y.K. Chembo, Opt. Lett. **41**, 3718 (2016)
61. A.B. Matsko, A.A. Savchenkov, S.-W. Huang, L. Maleki, Opt. Lett. **41**, 5102 (2016)
62. C. Bao, H. Taheri, L. Zhang, A. Matsko, Y. Yan, P. Liao, L. Maleki, A.E. Willner, J. Opt. Soc. Am. B **34**, 715 (2017)